Inorganic Chemistry

Article

pubs.acs.org/IC

Fe^{III} Bipyrrolidine Phenoxide Complexes and Their Oxidized Analogues

Linus Chiang,[†] Didier Savard,[†] Yuichi Shimazaki,[‡] Fabrice Thomas,[§] and Tim Storr*[,†]

[†]Department of Chemistry, Simon Fraser University, Burnaby, British Columbia V5A 1S6, Canada

[‡]College of Science, Ibaraki University, Bunkyo, Mito, 310-8512, Japan

[§]Département de Chimie Moléculaire, Chimie Inorganique Redox (CIRE), UMR-5250, Université Grenoble Alpes, BP 53, 38041 Grenoble Cedex 9, France

Supporting Information

ABSTRACT: Fe^{III} complexes of the symmetric (2*S*,2′*S*)-[*N*,*N*′-bis(1-(2-hydroxy-3,5-di-*tert*-butylphenylmethyl))]-2,2′-bipyrrolidine ($\mathbf{H_2L^1}$) and dissymmetric (2*S*,2′*S*)-[*N*,*N*′-(1-(2-hydroxy-3,5-di-*tert*-butylphenylmethyl))-2-(pyridylmethyl)]-2,2′-bipyrrolidine ($\mathbf{HL^2}$) ligands incorporating the bipyrrolidine backbone were prepared, and the electronic structure of the neutral and one-electron oxidized species was investigated. Cyclic voltammograms (CV) of $\mathbf{FeL^1Cl}$ and $\mathbf{FeL^2Cl_2}$ showed expected redox waves corresponding to the oxidation of phenoxide moieties to phenoxyl radicals, which was achieved by treating the complexes with 1 equiv of a suitable chemical oxidant. The clean conversion of the neutral complexes to their oxidized forms was monitored by UV−vis-NIR spectroscopy, where an intense $\pi-\pi^*$ transition characteristic of a phenoxyl radical emerged ($[\mathbf{FeL^1Cl}]^{+\bullet}$: 25 500 cm^{-1} (9000 M^{-1} cm^{-1}); $[\mathbf{FeL^2Cl_2}]^{+\bullet}$: 24 100 cm^{-1} (8300 M^{-1} cm^{-1}). The resonance Raman (rR) spectra of $[\mathbf{FeL^1Cl}]^{+\bullet}$ and $[\mathbf{FeL^2Cl_2}]^{+\bullet}$ displayed the characteristic phenoxyl radical ν_{7a} band at 1501 and 1504 cm^{-1}, respectively, confirming ligand-based oxidation. Electron paramagnetic resonance (EPR) spectroscopy exhibited a typical high spin Fe^{III} (S = 5/2) signal for the neutral complexes in perpendicular mode. Upon oxidation, a signal at $g \approx 9$ was observed in parallel mode, suggesting the formation of a spin integer system arising from magnetic interactions between the high spin Fe^{III} center and the phenoxyl radical. Density functional theory (DFT) calculations further supports this formulation, where weak antiferromagnetic coupling was predicted for both $[\mathbf{FeL^1Cl}]^{+\bullet}$ and $[\mathbf{FeL^2Cl_2}]^{+\bullet}$.

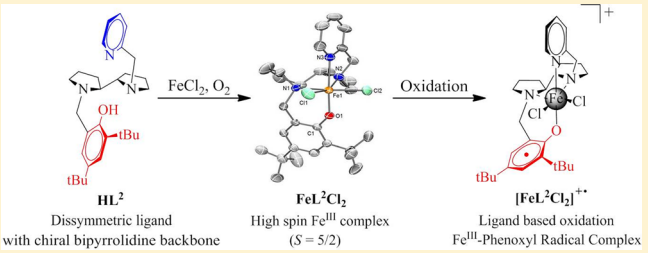

1. INTRODUCTION

Correlating the electronic structure and reactivity of inorganic entities is of considerable interest, both in nature[1] and in synthetic model systems.[2] In certain metalloenzyme systems, the transition metal functions in a cooperative manner with a redox active ligand to promote multielectron reactions. One such enzyme is galactose oxidase,[1,3] which catalyzes the two-electron oxidation of primary alcohols to aldehydes. To drive this chemistry, galactose oxidase utilizes two one-electron redox cofactors: a Cu center and a post-translationally modified tyrosine residue. This modification, in the form of a Tyr-Cys cross-link, is a key determinant in lowering the $Tyr^{\bullet}$/Tyr redox potential, leading to stabilization of the radical resting state of the enzyme. Numerous structural and functional synthetic models of galactose oxidase have been studied, owing to the simplicity of the active site.[4] Other notable examples include heme proteins, such as cytochrome P_{450}, catalase, and peroxidase, which form a Fe^{IV}-oxo heme radical cation (also known as Compound I) to promote oxidation reactions.[5]

Depending on the energies of the redox-relevant orbitals, complexes with pro-radical ligands ($[M^{n+}L]$) can undergo ligand-based ($[M^{n+}L^{\bullet}]^{+}$) or metal based ($[M^{(n+1)}L]^{+}$) oxidation. One class of ligand that has been studied extensively for their cooperative capabilities in synthetic models are salen ligands (salen is a common abbreviation for N_2O_2 bis(Schiff base)-bis(phenolate) ligands).[6] These tetradentate ligands are attractive targets due to their relative ease of synthesis and their ability to form stable complexes with many metals in a variety of oxidation states, several of which are robust catalysts for organic transformations.[7] Importantly, many metallosalen complexes have been shown to exist in the $[M(Salen)^{\bullet}]^{+}$ electronic state upon oxidation, demonstrating the utility of salens as redox active ligands.[4a,6a,b,f,i,k,m,n,r,8] Specifically, Fe salen complexes have received significant attention as synthetic models of heme systems.[8,9] In certain cases, the ligand radical formed was found to be delocalized over the π system of the aromatic ring, generating a phenoxyl radical species. Numerous Fe^{III} phenoxide complexes have also been investigated and are capable of undergoing successive oxidations to afford multiple ligand radical species.[10]

The Fe complexes outlined above utilize a series of different amine backbones as starting materials, from macrocyclic[10a−c,11] to linear amines.[9d,10d,11,12] Of particular interest are chiral

Received: March 21, 2014
Published: May 9, 2014

   dx.doi.org/10.1021/ic500663x | *Inorg. Chem.* 2014, 53, 5810−5819

diamines, highlighted by Jacobsen's catalyst, a Mn^{III} salen that employs *trans*-1,2-cyclohexanediamine as the backbone. It was found that the chirality of the backbone can induce stereoselectivity during catalysis.[7a,d] However, it has also been shown that reduced bis-alkoxy ligands employing the cyclohexanediamine backbone bind metal ions as a mixture of diastereomers,[13] likely due to ligand flexibility. To this end, the use of a more constrained backbone, such as 2,2′-bipyrrolidine, has been shown to form metal complexes diastereospecifically.[14] As such, there have been an increasing number of catalysts reported that employ this backbone.[15] In particular, the recent use of Fe complexes incorporating the bipyrrolidine backbone for selective C−H oxidation and asymmetric epoxidation chemistry is impressive.[15b−e] However, reports of ligands with this backbone have been limited to symmetric structures, where the pendant arms are either both phenolates or both pyridines. Therefore, we aimed to synthesize the first example of dissymmetric Fe^{III} complexes using the 2,2′-bipyrrolidine scaffold with one redox active phenoxide and one pyridine donor appended onto the chiral backbone ($\mathbf{HL^2}$) and compare this to the symmetric Fe^{III} complex where both pendant arms are redox active phenoxides ($\mathbf{H_2L^1}$, Chart 1). We aimed to characterize the oxidized forms of these Fe complexes and in particular the generation and stability of ligand radical species. An improved understanding of the electronic signature of the ligand radical forms will inform future studies in oxidative catalysis.

Chart 1. Symmetric ($\mathbf{H_2L^1}$) and Dissymmetric ($\mathbf{HL^2}$) Ligands

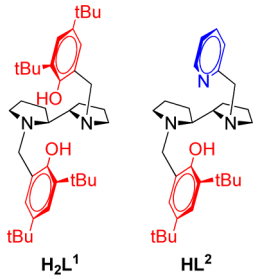

2. EXPERIMENTAL SECTION

2.1. Materials and Methods. All chemicals used were of the highest grade available and were further purified whenever necessary.[16] The aminium radical chemical oxidant $[N(C_6H_3Br_2)_3]^{+\bullet}[SbF_6]^-$ was synthesized according to published protocols.[17] 3,5-Di-*tert*-butyl-2-hydroxybenzyl bromide (**3**) was prepared from commercially available 2,4-di-*tert*-butylphenol in two steps by reported procedures.[18] Electronic spectra were obtained on a Cary 5000 spectrophotometer with a custom-designed immersion fiber-optic probe with variable path-length (1 and 10 mm; Hellma, Inc.). Constant temperatures were maintained by a dry ice/acetone bath. Solvent contraction was accounted for in all variable-temperature studies. Cyclic voltammetry (CV) was performed on a PAR-263A potentiometer, equipped with an Ag wire reference electrode, a platinum disk working electrode, and a Pt counter electrode with $^nBu_4NClO_4$ (0.1 M) solutions in CH_2Cl_2. Decamethylferrocene was used as an internal standard. Electrolysis was performed by using a PAR-273A potentiostat at −40 °C using a large Pt grid as the working electrode. Rotating disk electrode (RDE) voltammetry was performed to monitor electrochemical oxidation using a radiometer TCV101 speed control unit and a EDI 101 electrode. ^{1}H NMR spectra were recorded on a Bruker AV-500 instrument. Mass spectra (positive ion) were obtained on an Agilent 6210 TOP ESI-MS instrument. Elemental analyses (C, H, N) were performed by Mr. Farzad Haftbaradaran and Mr. Paul Mulyk at Simon Fraser University on a Carlo Erba EA1110 CHN elemental analyzer. All electron paramagnetic resonance (EPR) spectra were collected using a Bruker EMXplus spectrometer operating with a premiumX X-band microwave bridge and a dual mode resonant cavity (∼9.39 GHz in parallel mode, 9.63 GHz in perpendicular mode). Low temperature measurements of frozen solutions used an Oxford Instruments helium temperature-control system and continuous flow cryostats. Samples for X-band measurements were placed in 4 mm outer-diameter sample tubes with sample volumes of approximately 300 μL. Resonance Raman spectra were obtained on a MC-100DC spectrometer (Ritsu Oyo Kogaku) with a Beamlok Kr-ion laser (Spectra-Physics) for 406.7 nm excitation, a holographic supernoch filter (Kaiser Optical Systems), and Symphony CCD detector (HORIBA Jobin Yvon) cooled with liquid N_2. Spectra of solvated samples were collected in spinning cells (0.5 cm diameter, 330 rpm) at −50 °C at an excitation wavelength ν_{ex} = 406.7 nm (20 mW), 135° back scattering geometry, and 5 min data accumulation time. Peak frequencies were calibrated relative to indene standards (accurate to ±1 cm^{-1}).

2.2. X-ray Structure Determination. Single crystal X-ray crystallographic analysis of $\mathbf{FeL^1Cl}$ and $\mathbf{FeL^2Cl_2}$ was performed on a Bruker X8 APEX II diffractometer with graphite monochromated Mo−Kα radiation. A dark purple block ($\mathbf{FeL^1Cl{\cdot}MeCN}$) or dark blue prism ($\mathbf{FeL^2Cl_2{\cdot}CH_2Cl_2}$) crystal was mounted on a glass fiber. The data were collected at 293 ± 0.1 K to a maximum 2θ value of 55.0°. Data were collected in a series of ϕ and ω in 0.50° widths with 10.0 s exposures. The crystal-to-detector distance was 50 mm. The structure was solved by direct methods (SIR92)[19] and refined by least-squares procedures using CRYSTALS (v14.40b)[20] or ShelXle.[21] The materials crystallize with one molecule of solvent in the asymmetric unit. All non-hydrogen atoms were refined anisotropically. All C−H hydrogen atoms were placed in calculated positions but were not refined. All crystal structure plots were produced using ORTEP-3 and rendered with POV-Ray (v.3.6.2).[22] A summary of the crystal data and experimental parameters for structure determinations is given in Table 2. The structure of (*R*,*R*)-$\mathbf{FeL^2Cl_2}$ was solved in a unit cell of the space group P_{212121}, which is a part of a larger unit cell of the same space group.

2.3. Oxidation Protocol. Under an inert atmosphere at 198 K, 400 μL of a CH_2Cl_2 solution of the metal complex (4.6 mM) was diluted into 3.0 mL of CH_2Cl_2. Monitored by UV−vis-NIR, a saturated solution of $[NC_6H_3Br_2)_3]^{+\bullet}$ $[SbF_6]^-$ in CH_2Cl_2 was added in 20 μL additions resulting in clean conversion to the respective one-electron oxidized species.

2.4. Calculations. Geometry optimizations were performed using the Gaussian 09 program (Revision D.01),[23] the B3LYP functional,[24] and the 6-31G(d) basis set on all atoms. Frequency calculations at the same level of theory confirmed that the optimized structures were located at a minimum on the potential energy surface. Single point calculations for energetic analysis were performed with the B3LYP functional and the TZVP basis set of Ahlrichs on all atoms.[25] Broken-symmetry (BS) density functional theory (DFT) calculations were performed with the same functional and basis set.[26] The corresponding orbital transformation (COT) was used to determine the magnetic orbitals for the oxidized systems.[27] AOMix was used for determining atomic orbital compositions employing Mulliken population analysis.[28]

2.5. Synthesis. *2.5.1. (2S,2′S)-[N-(2-(Pyridylmethyl)]-2,2′-bipyrrolidine (2).* To a solution of (2*S*,2′*S*)-2,2′-bipyrrolidine (**1**) (500 mg, 3.6 mmol) in 1,2-dichloroethane (10 mL) was added K_2CO_3 (493 mg, 14.4 mmol), followed by 2-pyridinecarboxaldehyde (385 mg, 3.6 mmol). The reaction mixture was stirred at room temperature for 2 h and then filtered and concentrated *in vacuo*. The product was dissolved in anhydrous EtOH (30 mL), followed by the addition of 10% Pd/C (150 mg). The reaction mixture was stirred under a H_2 atmosphere for 3 days. This mixture was filtered over Celite, and the filtrate was concentrated *in vacuo* to afford a yellow oil. The crude product was subject to flash column chromatography using neutral alumina as the stationary phase (eluent: 20:1 CH_2Cl_2/MeOH) to afford a pale yellow oil that crystallizes over time as the amine **2**. Yield: 645 mg, 81%. ^{1}H

dx.doi.org/10.1021/ic500663x | Inorg. Chem. 2014, 53, 5810−5819

NMR ($CDCl_3$, 500 MHz): δ = 8.46−8.48 (ddd, 1H, Ar−H, J = 6.2, 2.0, 1.0), 7.65−7.69 (dt, 1H, Ar−H, J = 9.6, 2.2), 7.19−7.22 (m, 1H, Ar−H), 7.18 (d, 1H, Ar−H, J = 9.8), 4.11 (d, 1H, Ar−CH, J = 19.7), 3.85 (d, 1H, Ar−CH, J = 19.7), 3.49−3.55 (m, 1H, N−CH), 3.40−3.46 (m, 1H, N−CH), 3.11−3.21 (m, 2H, N−CH), 2.93−2.98 (m, 1H, N−CH), 2.63−2.69 (m, 1H, CH), 1.98−2.13 (m, 3H, CH), 1.84−1.94 (m, 3H, CH), 1.53−1.64 (m, 2H, CH); MS (ESI): m/z (%): 232.1798 (100) [**2** + H]$^+$.

*2.5.2. (2S,2′S)-[N,N′-(1-(2-Hydroxy-3,5-di-tert-butylphenylmethyl))-2-(pyridylmethyl)]-2,2′-bipyrrolidine (**HL^2**).* To a solution of amine **2** (661 mg, 2.9 mmol) in MeCN (15 mL) was added K_2CO_3 (395 mg, 3.1 mmol), followed by a solution of benzyl bromide **3** (855 mg, 2.9 mmol) in MeCN (20 mL) dropwise at 0 °C. The resultant mixture was warmed to room temperature, stirred for 16 h, and then filtered, and the filtrate was concentrated *in vacuo*. The crude product was subjected to flash column chromatography using silica gel as the stationary phase (eluent: 20:1 CH_2Cl_2/MeOH) to afford a pale yellow solid of ligand **HL^2**. Yield: 855 mg, 67%. ^{1}H NMR ($CDCl_3$, 500 MHz): δ = 8.52−8.53 (d, 1H, Ar−H, J = 4.3), 7.61−7.64 (dt, 1H, Ar−H, J = 7.6, 0.9), 7.38 (d, 1H, Ar−H, J = 7.7), 7.19 (d, 1H, Ar−H, J = 1.8), 7.13−7.15 (dd, 1H, Ar−H, J = 6.5, 5.5), 6.83 (d, 1H, Ar−H, J = 1.5), 4.22 (d, 1H, Ar−CH, J = 13.4), 4.03 (d, 1H, Ar−CH, J = 14.1), 3.50 (d, 1H, Ar−CH, J = 14.1), 3.39 (d, 1H, Ar−CH, J = 13.5), 3.03−3.07 (m, 1H, N−CH), 2.97−3.00 (m, 1H, N−CH), 2.88−2.91 (m, 1H, N−CH), 2.74−2.78 (m, 1H, N−CH), 2.20−2.29 (m, 2H, N−CH), 1.68−1.98 (m, 8H, CH), 1.40 (s, 9H, *t*-Bu), 1.27 (s, 9H, *t*-Bu); MS (ESI): m/z (%): 450.3579 (100) [**HL^2** + H]$^+$; elemental analysis: calculated (found) for $C_{29}H_{43}N_3O$·0.1 CH_2Cl_2: C 76.29, H 9.50, N 9.17; Found: C 76.57, H 9.51, N 9.25.

*2.5.3. Synthesis of **FeL^{1}Cl**.* To a solution of ligand **H$_2$L^1** (340 mg, 0.6 mmol) in MeCN (15 mL) was added $FeCl_2$ (77 mg, 0.6 mmol) under aerobic conditions. The solution immediately turned purple upon addition and was stirred at room temperature for 2 h, after which it was concentrated *in vacuo*. The purple powder was recrystallized under an inert atmosphere by slow evaporation of a concentrated solution of **FeL^{1}Cl** in MeCN to afford dark purple crystals. Yield: 143 mg, 36%. MS (HRMS): m/z: 666.3599; elemental analysis: calculated (%) for $C_{38}H_{58}N_2O_2ClFe$·MeCN: C 67.88, H 8.69, N 6.10; found: C 67.82, H 8.83, N 6.24. Solution magnetic moment (^{1}H Evan's Method): μ_{eff} = 5.98.

*2.5.4. Synthesis of **FeL^{2}Cl$_2$**.* To a solution of ligand **HL^2** (110 mg, 0.2 mmol) in MeCN (4 mL) was added $FeCl_2$ (31 mg, 0.2 mmol) under aerobic conditions. The solution immediately turned dark blue upon addition and was stirred at room temperature for 2 h, after which it was concentrated *in vacuo*. The blue powder was recrystallized under an inert atmosphere by the diffusion of diethyl ether into a concentrated solution of **FeL^{2}Cl$_2$** in CH_2Cl_2 to afford dark blue crystals. Yield: 89 mg, 63%. MS (HRMS): m/z: 574.2041; elemental analysis: calculated (%) for $C_{29}H_{42}N_3OCl_2Fe$·1.2 CH_2Cl_2/C 53.55, H 6.61, N 6.20; found: C 53.33, H 6.64, N 6.30. Solution magnetic moment (^{1}H Evan's Method): μ_{eff} = 5.89.

3. RESULTS AND DISCUSSION

3.1. Synthesis and Solid State Characterization of Ligands and Complexes. (*S*,*S*)-**H$_2$L^1** was prepared by reported methods.[14b,c] The synthetic scheme of the dissymmetric ligand (*S*,*S*)-**HL^2** is presented in Scheme 1. (*S*,*S*)-**HL^2** was prepared starting with the condensation of commercially available chiral (2*S*,2′*S*)-2,2′-bipyrrolidine (**1**) with 2-pyridinecarboxaldehyde, where the formation of the aminal intermediate was confirmed by ^{1}H NMR, but was not isolated due to its limited stability. This product was immediately subjected to hydrogenation conditions to form amine **2**, which was then reacted with 1 equiv of benzyl bromide **3** to afford dissymmetric ligand (2*S*,2′*S*)-[*N*,*N*′-(1-(2-hydroxy-3,5-di-*tert*-butylphenylmethyl))-2-(pyridylmeth-yl)]-2,2′-bipyrrolidine ((*S*,*S*)-**HL^2**).

Scheme 1. Synthetic Scheme for Dissymmetric Ligand HL^2[a]

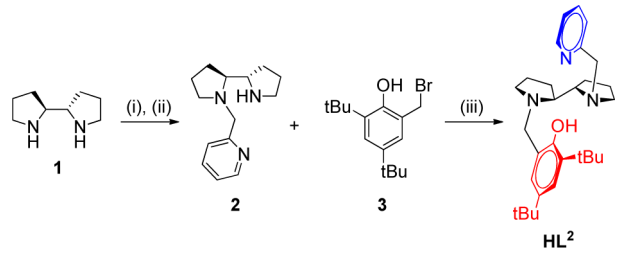

[a](i) 2-Pyridinecarboxaldehyde, 1,2-dichloroethane; (ii) H_2, 10% Pd/C, EtOH; (iii) K_2CO_3, MeCN.

(*S*,*S*)-**FeL^{1}Cl** and (*S*,*S*)-**FeL^{2}Cl$_2$** were prepared by treating an acetonitrile solution of the corresponding ligand with $FeCl_2$ in air, and the metal complexes were isolated in bulk following the removal of solvents *in vacuo*. Recrystallization of (*S*,*S*)-**FeL^{1}Cl** (slow evaporation of acetonitrile) and (*S*,*S*)-**FeL^{2}Cl$_2$** (slow diffusion of diethyl ether into dichloromethane) afforded X-ray suitable crystals in moderate yield. Solution magnetic susceptibility measurements (^{1}H Evan's method) revealed that (*S*,*S*)-**FeL^{1}Cl** (μ_{eff} = 5.98) and (*S*,*S*)-**FeL^{2}Cl$_2$** (μ_{eff} = 5.89) both contain a high spin, S = 5/2 Fe^{III} center. The (*R*,*R*) analogues of these complexes were prepared in a similar manner, starting with (2*R*,2′*R*)-2,2′-bipyrrolidine (Figures S1 and S2, Supporting Information). For the remainder of the manuscript, **FeL^{1}Cl** and **FeL^{2}Cl$_2$** refers to the (*S*,*S*) complexes.

3.2. X-ray Analysis of FeL^{1}Cl and FeL^{2}Cl$_2$. The molecular structures of **FeL^{1}Cl** and **FeL^{2}Cl$_2$** are presented in Figure 1 and

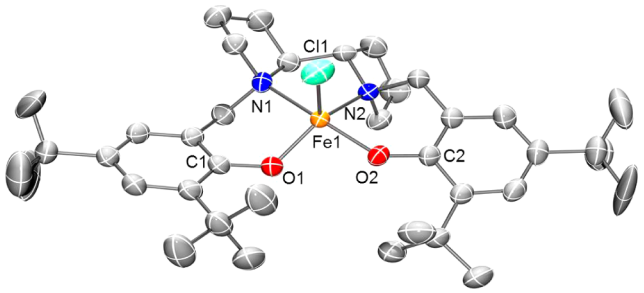

Figure 1. ORTEP plot of **FeL^{1}Cl** (50% probability) using POV-Ray, excluding hydrogen atoms. Selected interatomic distances [Å] and angles [°]: Fe(1)−O(1): 1.865, Fe(1)−O(2): 1.866, Fe(1)−N(1): 2.246, Fe(1)−N(2): 2.132, Fe(1)−Cl(1): 2.217, C(1)−O(1): 1.333, C(2)−O(2): 1.317; angles: N(1)−Fe(1)−O(1): 88.6, N(1)−Fe(1)−N(2): 78.0, N(2)−Fe(1)−O(2): 86.2, O(1)−Fe(1)−O(2): 92.9, N(1)−Fe(1)−O(2): 159.1, N(2)−Fe(1)−O(1): 134.8, N(1)−Fe(1)−Cl(1): 96.1, N(2)−Fe(1)−Cl(1): 109.0, O(1)−Fe(1)−Cl(1): 115.4, O(2)−Fe(1)−Cl(1): 102.1.

Figure 2 respectively, and select crystallographic data are shown in Table 1. The solid state structure for **FeL^{1}Cl** exhibits a slightly distorted square pyramidal geometry with the expected N_2O_2 coordination sphere from the ligand and an apical chloride ligand, affording an overall neutral complex. The Fe-amine (Fe1−N1:2.245 Å, Fe1−N2:2.131 Å) bond distances are in line with other structurally similar 5-coordinate diamine-bisphenoxide Fe^{III} complexes.[9d,11,12] Interestingly, the slight difference in bond distances between the metal ion and the two bipyrrolidine amine nitrogens have also been observed for other square pyramidal bipyrrolidine complexes.[14c,29] This is possibly a result of the sterically demanding ortho *tert*-butyl moieties, which distorts the ligand donors from an ideal square pyramidal

dx.doi.org/10.1021/ic500663x | Inorg. Chem. 2014, 53, 5810−5819

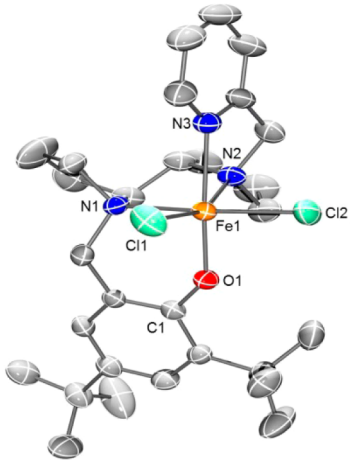

Figure 2. ORTEP plot of FeL^2Cl_2 (50% probability) using POV-Ray, excluding hydrogen atoms and solvent. Selected interatomic distances [Å] and angles [°]: Fe(1)−N(1): 2.243, Fe(1)−N(2): 2.253, Fe(1)−N(3): 2.289, Fe(1)−O(1): 1.876, Fe(1)−Cl(1): 2.321, Fe(1)−Cl(2): 2.314, C(1)−O(1): 1.338; angles: N(1)−Fe(1)−Cl(2): 169.4, N(2)−Fe(1)−Cl(1): 158.2, N(3)−Fe(1)−O(1): 170.6, N(1)−Fe(1)−N(2): 77.2, N(2)−Fe(1)−Cl(2): 92.3, Cl(2)−Fe(1)−Cl(1): 99.5, Cl(1)−Fe(1)−N(1): 90.9, N(3)−Fe(1)−N(2): 72.7, N(2)−Fe(1)−O(1): 97.9, O(1)−Fe(1)−Cl(1): 99.6, Cl(1)−Fe(1)−N(3): 89.7, N(3)−Fe(1)−Cl(2): 86.6, Cl(2)−Fe(1)−O(5): 93.5, O(1)−Fe(1)−N(1): 86.5, N(1)−Fe(1)−N(3): 91.7.

geometry. As expected, these bond distances are longer than the Fe−N_{imine} bond distance for Fe(Salen)Cl (2.102, 2.087 Å).[30] The Fe1−O1 and Fe1−O2 bond distances (1.864, 1.866 Å) are similar to that of Fe−$O_{phenoxide}$ in Fe(Salen)Cl (1.882 Å),[30] while the C1−O1 bond distance is also typical of a phenoxide moiety. The donor atoms in **FeL^1Cl** are forced from the mean equatorial plane by 0.21−0.22 Å, and the metal center is positioned 0.54 Å above this plane. These values are greater than those observed in a similar diamine-bisphenoxide complex,[9d,12] suggesting a stronger distortion at the metal center. This was reflected in the calculated trigonality index[31] τ of 0.41, which was defined by the equation $\tau = (\beta - \alpha)/60$, where β is the N1−Fe1−O2 angle and α is the N2−Fe1−O1 angle. Perfectly trigonal bipyramidal and square pyramidal complexes have τ values of 1 and 0, respectively. The larger τ value observed for **FeL^1Cl**, in comparison to other 5-coordinate diamine-bisphenoxide Fe^{III} complexes with backbones such as ethylenediamine ($\tau = 0.31$)[9d,12] or homopiperazine ($\tau = 0.20$)[11] is likely a result of the more rigid bipyrrolidine, leading to a more distorted metal center.

The solid state structure of **FeL^2Cl_2** exhibits a slightly distorted octahedral geometry with the expected N_3O coordination sphere of the ligand and two chloride ligands to afford an overall neutral complex. The ligand, featuring a (*S*,*S*)-bipyrrolidine backbone, coordinates to the metal in a Λ helical manner, as previously observed for other metal complexes employing this enantiomer as the backbone.[14b] Conversely, the metal center is coordinated in a Δ helical manner when the enantiomer of this ligand was prepared using (*R*,*R*)-bipyrrolidine as the backbone (Figure S2, Supporting Information), demonstrating the induction of chirality from ligand to metal depending on backbone stereochemistry.[14c] The Fe−N_{amine} bond distances are similar to those found for **FeL^1Cl** and are significantly longer than reported Fe−N_{imine} bond distances for Fe(Salen)Cl.[30a] The Fe1−O1 and C1−O1 bond distances are similar to those in **FeL^1Cl**, supporting the Fe^{III}-phenoxide formulation. Interestingly, the two Cl ligands occupy a *cis*-α conformation; it has been shown that labile ligands in this orientation are critical to catalytic activity and stereoselectivity.[15b,c]

Table 2. Selected Crystallographic Data for FeL^1Cl and FeL^2Cl_2

	FeL^1Cl	$FeL^2Cl_2{\cdot}CH_2Cl_2$
formula	$C_{38}H_{58}ClN_2O_2Fe$	$C_{30}H_{44}Cl_4N_3OFe$
formula weight	666.16	660.33
space group	H_3	P_{212121}
a (Å)	27.55(2)	9.0064(9)
b (Å)	27.55(2)	14.6395(15)
c (Å)	12.754(11)	24.409(2)
α (deg)	90	90
β (deg)	90	90
γ (deg)	120	90
V [Å^3]	8382(16)	3218.3(6)
Z, D_{calc} [g/cm^3]	9	4
T (K)	296	296
ρ_{calcd} (g cm^{-3})	1.188	1.363
λ (Å)	0.710 73	0.710 73
μ (cm^{-1})	0.510	0.828
R indices[a] with $I > 2\sigma(I)$ (data)	0.0424	0.0304
wR_2	0.1096	0.0767
R_1	0.0488	0.0361
goodness-of-fit on F^2	1.015	1.055

[a]Goodness-of-fit on *F*.

3.3. Theoretical Analysis of FeL^1Cl and FeL^2Cl_2. DFT calculations were carried out on neutral **FeL^1Cl** and **FeL^2Cl_2**. In both cases, a high spin $S = 5/2$ Fe^{III} center was predicted to be the lowest in energy, in line with solution state magnetic data. The $S = 5/2$ high spin state was favored over the $S = 3/2$ intermediate spin state (**FeL^1Cl**: +15 kcal/mol; **FeL^2Cl_2**: +18 kcal/mol) and the $S = 1/2$ low spin state (**FeL^1Cl**: +27 kcal/mol; **FeL^2Cl_2**: +22 kcal/mol). With the exception of the Fe−N_{amine} bonds, which can be overestimated by DFT calculations,[32] optimized structures of **FeL^1Cl** and **FeL^2Cl_2**

Table 1. Experimental and Calculated (in Parentheses) Coordination Sphere Metrical Parameters for the Fe Complexes (in Å)

			amines						
complex	Fe1−O1	Fe1−O2	Fe1−N1	Fe1−N2	Fe1−N3	Fe1−Cl1	Fe1−Cl2	C1−O1	C2−O2
FeL^1Cl	1.865	1.866	2.246	2.132		2.217		1.333	1.317
	(1.857)	(1.865)	(2.334)	(2.225)		(2.274)		(1.340)	(1.335)
$[FeL^1Cl]^+$	(1.824)	(2.010)	(2.219)	(2.227)		(2.236)		(1.347)	(1.278)
FeL^2Cl_2	1.876		2.243	2.253	2.289	2.321	2.314	1.338	
	(1.859)		(2.340)	(2.341)	(2.335)	(2.320)	(2.314)	(1.332)	
$[FeL^2Cl_2]^+$	(2.014)		(2.337)	(2.289)	(2.202)	(2.268)	(2.259)	(1.276)	

dx.doi.org/10.1021/ic500663x | *Inorg. Chem.* 2014, 53, 5810−5819

using the B3LYP functional and 6-31G(d) basis set are in good agreement with the solid state data, predicting coordination bond lengths to within ±0.06 Å (Table 1). In addition, the slight asymmetry in the coordination sphere for **FeL^{1}Cl** observed in the X-ray structure was also well predicted, where the bulky ortho *tert*-butyl groups forces the two phenoxide moieties out of the plane from one another. The trigonality index of this optimized structure is 0.23, further supporting a strongly distorted square pyramidal geometry around the metal center. Of note, a hydrogen bonding interaction was also predicted between the Cl atom and a benzylic proton (Cl···H: 2.73 Å), which may further contribute to the asymmetric coordination sphere.

3.4. Electrochemistry. Redox processes for **FeL^{1}Cl** and **FeL^{2}Cl$_2$** were probed by cyclic voltammetry (CV) in CH_2Cl_2 by using tetra-*n*-butyl-ammonium perchlorate ($^nBu_4NClO_4$) as the supporting electrolyte (Figure 3). The redox potentials

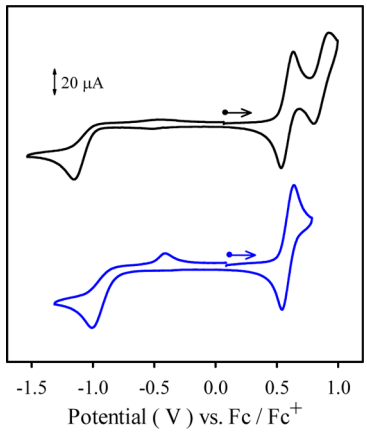

Figure 3. Cyclic voltammogram of **FeL^{1}Cl** (black) and **FeL^{2}Cl$_2$** (blue). Conditions: 2.5 mM complex, 0.1 M $^nBu_4NClO_4$, scan rate 100 mV s^{-1}, CH_2Cl_2, 233 K.

versus ferrocenium/ferrocene (Fc^+/Fc) are reported in Table 3. An irreversible reduction wave was observed for both **FeL^{1}Cl** and **FeL^{2}Cl$_2$**, corresponding to a metal-based reduction from Fe^{III} to Fe^{II} in line with previous reports.[10b,e] We examined whether loss of a chloride ligand upon reduction leads to the irreversible redox process; however, examining the reduction using a large excess of chloride (Et_4NCl as the supporting electrolyte) did not improve the reversibility of this redox wave. This result is in contrast to reported 5- or 6-coordinate Fe^{III} amine-phenolate complexes which display reversible Fe^{III}/Fe^{II} redox waves and is likely due to structural reorganization upon reduction in this study.[10b,e] A quasi-reversible one-electron redox process was observed for **FeL^{2}Cl$_2$** at 0.59 V vs F_c^+/F_c, which was assigned to ligand-centered oxidation from phenoxide to the corresponding phenoxyl radical species based on comparison to the CV of the ligand **HL^2** (Figure S3, Supporting Information) and is further confirmed by resonance Raman studies (*vide infra*). A second irreversible oxidative process for **FeL^{2}Cl$_2$** was observed at ca. 1.4 V at the limit of the solvent window (Figure S4, Supporting Information).

In the case of **FeL^{1}Cl**, two quasi-reversible one-electron oxidation waves were observed, with the first wave assigned to a ligand-centered oxidation similarly to **FeL^{2}Cl$_2$**. The nature of the second oxidative wave is currently under investigation. A structurally analogous bisphenoxide Fe^{III} salen complex reported by Fujii et al. exhibited similar electrochemical behavior, where two one-electron ligand-based oxidative waves were observed at 0.85 and 0.96 V vs Fc^+/Fc.[8] **FeL^{1}Cl** displays considerably lower oxidation potentials in comparison to Fe(Salen)Cl, likely due to the increased electron-donating nature of the amine moieties in comparison to imines.

The electrochemical data for Fe(Salen)Cl,[8] and several reports of Fe^{III}/Fe^{IV} couples at >0.9 V vs Fc^+/Fc,[33] suggest that the second oxidative wave of **FeL^{1}Cl** is likely a ligand-based oxidation. No further oxidation waves were observed when scanning toward more oxidizing potentials (Figure S5, Supporting Information). As such, the difference between the first and second redox potentials (ΔE_{ox}) can provide insight regarding the amount of electronic coupling between the two redox-active phenoxide moieties, as well as the degree of electronic delocalization upon oxidation. Theoretically, in the absence of electronic coupling, a symmetric complex with two redox active moieties should exhibit two redox processes separated by $\Delta E_{ox} = [RT/F] \ln 4)$,[34] which is often observed as a single, two-electron redox couple due to limited resolution. This was not observed experimentally (Figure 3). The relative stability toward comproportionation of the monooxidized species (K_c) can be described by eqs 1−3 using ΔE_{ox}.

$$[ML] + [ML^{\bullet\bullet}] \rightleftharpoons 2[ML^{\bullet}] \quad (1)$$

$$K_c = \frac{[ML^{\bullet}]^2}{[ML][ML^{\bullet\bullet}]} \quad (2)$$

$$K_c = \exp\left(\frac{\Delta E_{ox} F}{RT}\right) \quad (3)$$

The values of K_c and ΔE_{ox} for **FeL^{1}Cl**, reported in Table 3, suggest moderate coupling between the two redox-active phenoxides. This pattern has also been observed for the Cu complex of **H$_2$L^1**, which exhibits a ΔE_{ox} of 0.14 V and a K_c of 1.1×10^3.[35] In addition, Fujii et al. have hypothesized that the increased charge of the metal center (M^{III} vs M^{II}) leads to a contraction of the metal d orbital manifold, which in turn limits delocalization of the ligand radical due insufficient orbital overlap.[6k] This is also in good agreement with our experimental results.

3.5. Electronic Spectroscopy. The electronic absorption spectra of **FeL^{1}Cl** and **FeL^{2}Cl$_2$** are typical of high spin Fe^{III} phenoxide complexes (Figure 4).[11,12] A characteristic phenoxide to Fe^{III} charge transfer band was observed in the visible

Table 3. Redox Potentials of Fe Complexes versus Fc^+/Fc[a] Peak to Peak Separation in Parentheses

compound	E_{red} (V)	$E_{1/2}{}^1$ (V)	$E_{1/2}{}^2$ (V)	ΔE_{ox} ($E_{1/2}{}^2 - E_{1/2}{}^1$) (V)	K_c (233 K)
FeL^{1}Cl	−1.16 (irr.)	0.59 (0.10)	0.86 (0.13)	0.27	6.9×10^5
Fe(Salen)Cl[b]		0.85	0.96	0.11	2.4×10^2
FeL^{2}Cl$_2$	−1.01 (irr.)	0.59 (0.10)			

[a]Peak to peak difference for Fc^+/Fc couple at 233 K is 0.07 V. [b]Ref 8.

dx.doi.org/10.1021/ic500663x | *Inorg. Chem.* 2014, 53, 5810−5819

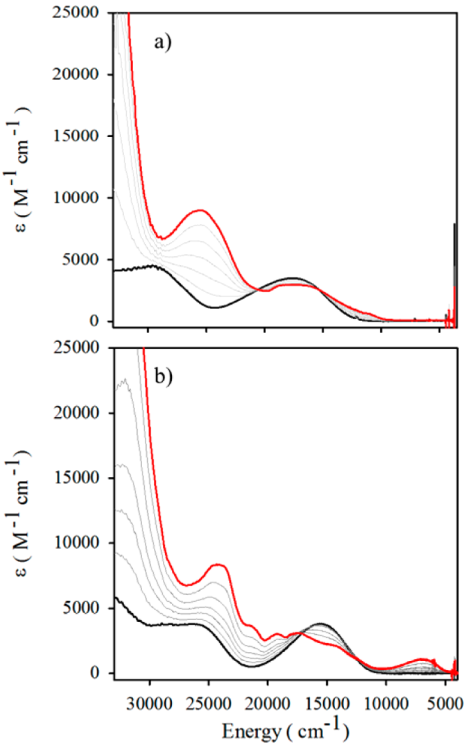

Figure 4. Electronic spectra of (a) $\mathbf{FeL^1Cl}$ (black), $[\mathbf{FeL^1Cl}]^{+\bullet}$ (red), and (b) $\mathbf{FeL^2Cl_2}$ (black) and $[\mathbf{FeL^2Cl_2}]^{+\bullet}$ (red) in CH_2Cl_2 at 198 K. Intermediate gray lines measured during the oxidation titration with $[N(C_6H_3Br_2)_3]^{+\bullet}[SbF_6]^-$.

region ($\mathbf{FeL^1Cl}$: 17 600 cm^{-1} (3500 M^{-1} cm^{-1})); $\mathbf{FeL^2Cl_2}$: 15 500 cm^{-1} (3800 M^{-1} cm^{-1})).[10b] The broad feature at higher energies is tentatively assigned to an amine to Fe^{III} charge transfer band.[10a,b]

Chemical oxidation using aliquots of the aminium radical oxidant $[N(C_6H_3Br_2)_3]^{+\bullet}[SbF_6]^-$ (E_{ox} = 1.1 V vs F_c^+/F_c in CH_2Cl_2) under an inert atmosphere at 198 K resulted in new spectra with isosbestic points ($\mathbf{FeL^1Cl}$: 20 600 and 15 300 cm^{-1}; $\mathbf{FeL^2Cl_2}$: 12 400 cm^{-1}), suggesting direct conversion of the neutral to the oxidized species. Substantial changes were observed upon oxidation, most notably the appearance of a new and intense band in the visible region ($[\mathbf{FeL^1Cl}]^{+\bullet}$: 25 500 cm^{-1} (9000 M^{-1} cm^{-1}); $[\mathbf{FeL^2Cl_2}]^{+\bullet}$: 24 100 cm^{-1} (8300 M^{-1} cm^{-1})), which was assigned to a $\pi-\pi^*$ transition of a phenoxyl radical species as previously observed for other phenoxyl radical-containing compounds.[10b] In addition, a bathochromic shift and decrease in the intensity of the phenoxide to Fe^{III} CT band was also observed ($\mathbf{FeL^1Cl}$: 17 600 cm^{-1} (3500 M^{-1} cm^{-1}); $[\mathbf{FeL^1Cl}]^{+\bullet}$: 16 700 cm^{-1} (2800 M^{-1} cm^{-1}); ($\mathbf{FeL^2Cl_2}$: 15500 cm^{-1} (3800 M^{-1} cm^{-1}); $[\mathbf{FeL^2Cl_2}]^{+\bullet}$: 14 400 cm^{-1} (2100 M^{-1} cm^{-1})). A similar pattern of these bands has been observed for an analogous Fe^{III}-phenoxyl radical complex.[10b] Half-lives at room temperature ($[\mathbf{FeL^1Cl}]^{+\bullet}$: $t_{1/2}$ = 6 h; $[\mathbf{FeL^2Cl_2}]^{+\bullet}$: $t_{1/2}$ = 12 min) precluded isolation of the oxidized species in the solid state for X-ray analysis.

3.6. Resonance Raman Spectroscopy. Resonance Raman spectroscopy (rR) of complexes $\mathbf{FeL^1Cl}$ and $\mathbf{FeL^2Cl_2}$, and their one-electron oxidized forms $[\mathbf{FeL^1Cl}]^{+\bullet}$ and $[\mathbf{FeL^2Cl_2}]^{+\bullet}$, were carried out at the excitation wavelength of 406.7 nm (Figure 5). The rR spectra exhibit a new peak upon oxidation: ($[\mathbf{FeL^1Cl}]^{+\bullet}$: 1504 cm^{-1}; $[\mathbf{FeL^2Cl_2}]^{+\bullet}$: 1501 cm^{-1}), which we tentatively assign as the phenoxyl radical ν_{7a} band.

Table 4. Spectroscopic Properties of the Fe Complexes in CH_2Cl_2 Solution[a]

complex	λ_{max}, cm^{-1} ($\varepsilon \times 10^3$, M^{-1} cm^{-1})
$\mathbf{FeL^1Cl}$	29300 br (4.4), 17600 (3.5)
$[\mathbf{FeL^1Cl}]^{+\bullet}$	25500 (9.0), 18700 sh (2.9), 16700 (2.8), 11100 w (0.52)
$\mathbf{FeL^2Cl_2}$	25800 br (3.7), 15500 br (3.8)
$[\mathbf{FeL^2Cl_2}]^{+\bullet}$	24100 (8.3), 21500 (3.6), 19200 (3.0), 17500 (3.1), 14400 (2.1), 12600 sh (1.2), 6900 (1.0)

[a]Conditions: 0.6 mM for $\mathbf{FeL^1Cl}$ and $\mathbf{FeL^2Cl_2}$, 0.4 mM for $[\mathbf{FeL^1Cl}]^{+\bullet}$ and $[\mathbf{FeL^2Cl_2}]^{+\bullet}$, CH_2Cl_2, 198 K.

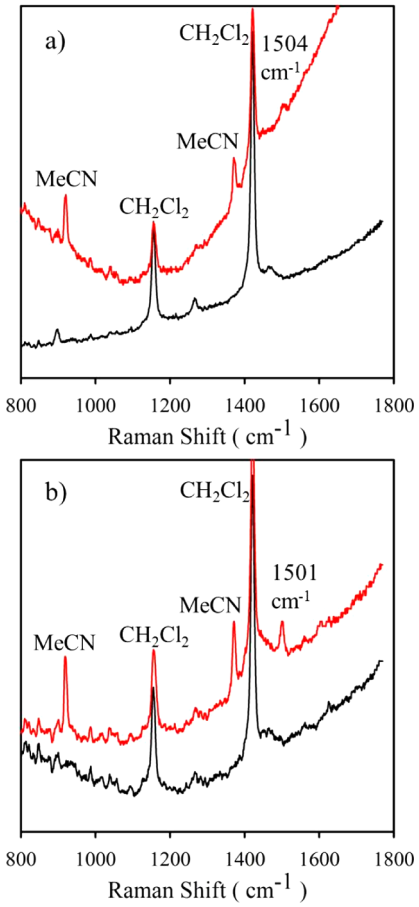

Figure 5. Resonance Raman (rR) spectra of (a) $\mathbf{FeL^1Cl}$ (black), $[\mathbf{FeL^1Cl}]^{+\bullet}$ (red); (b) $\mathbf{FeL^2Cl_2}$ (black), $[\mathbf{FeL^2Cl_2}]^{+\bullet}$ (red). The rR spectrum for the neutral complexes were collected in CH_2Cl_2, and their one-electron oxidized forms in 10:1 CH_2Cl_2/MeCN mixture. λ_{ex} = 406.7 nm, T = 223 K.

This observation suggests a ligand-based oxidation, further confirming the formation of Fe^{III}-phenoxyl radical species for both complexes. A similar series of bands has been observed in the rR spectrum of a related Fe^{III}-phenoxyl radical complex.[10b,36] It should be noted that the phenoxyl radical ν_{8a} band, which is expected to be found at ca. 1600 cm^{-1}, could not be detected due to significant fluorescence of the sample (beyond 1600 cm^{-1}).

3.7. Continuous Wave X-band Electron Paramagnetic Resonance. The perpendicular mode X-band EPR spectra of $\mathbf{FeL^1Cl}$ and $\mathbf{FeL^2Cl_2}$, and their one-electron oxidized forms $[\mathbf{FeL^1Cl}]^{+\bullet}$ and $[\mathbf{FeL^2Cl_2}]^{+\bullet}$, were collected at 10 K in CH_2Cl_2 with 0.1 M $^nBu_4NClO_4$ (Figures S6a and S7, Supporting Information). The EPR spectrum of $\mathbf{FeL^1Cl}$ display resonances

dx.doi.org/10.1021/ic500663x | Inorg. Chem. 2014, 53, 5810−5819

at g effective (g_{eff}) values of 2, 3.6, 4.3, 4.9, and 9.4 (Figure 6a). These features are consistent with a high-spin (S = 5/2) Fe^{III}

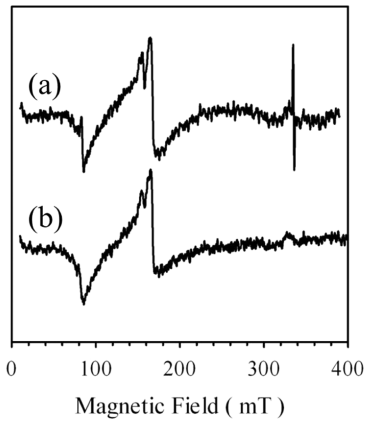

Figure 6. Parallel mode X-Band EPR spectrum of (a) 0.5 mM solution of electrochemically generated $[\mathbf{FeL^1Cl}]^{+\bullet}$ in CH_2Cl_2 with 0.1 M $^nBu_4NClO_4$. Conditions: Frequency, 9.385 GHz; power: 20.8 mW and (b) 0.5 mM solution of electrochemically generated $[\mathbf{FeL^2Cl_2}]^{+\bullet}$ at 0.5 mM in CH_2Cl_2 (containing 0.1 M $^nBu_4NClO_4$). Conditions: Frequency, 9.390 GHz; power, 8.4 mW; modulation frequency, 100 kHz; amplitude, 1 mT; T = 10 K.

center, where $|D| \gg h\nu$, as commonly observed for such complexes. This spectrum was analyzed using rhombograms, which represents the g_{eff} of the three Kramers' doublets $|\pm1/2>$, $|\pm3/2>$, $|\pm5/2>$ as a function of rhombicity E/D. The E/D ratio of 0.20 for $\mathbf{FeL^1Cl}$ signifies medium-to-strong rhombic distortions and compares well with a structurally similar complex.[9d] The EPR spectrum of $\mathbf{FeL^2Cl_2}$ in CH_2Cl_2 is markedly different in comparison to $\mathbf{FeL^1Cl}$ (Figure S7, Supporting Information). A dominant signal observed at g = 4.3 indicates larger rhombicity, which was reflected in the E/D value of 0.33 and is expected for an octahedral high spin Fe^{III} complex. Electrochemical oxidation of $\mathbf{FeL^1Cl}$ to $[\mathbf{FeL^1Cl}]^{+\bullet}$ induces quenching of the Fe^{III} EPR signal (ca. 90%), likely reflecting antiferromagnetic coupling between the radical and Fe^{III} center (Figure S6a, Supporting Information). In addition, the appearance of a sharp new signal at g = 2.00 indicates a minor uncoupled phenoxyl radical species (Figures S6a and S6b, Supporting Information); theoretical calculations predict elongation of the Fe−O bond upon oxidation to the ligand radical (*vide infra*). Electrochemical oxidation of $\mathbf{FeL^2Cl_2}$ to $[\mathbf{FeL^2Cl_2}]^{+\bullet}$ also results in quenching of the Fe^{III} EPR signal (ca. 65%); however, no significant signal at g = 2.00 was observed for this derivative (Figure S7, Supporting Information).

Due to the presence of the prominent signal at g = 4.3 (likely arising from a high spin Fe^{III} contaminant) that superimposes on the spectrum of $[\mathbf{FeL^1Cl}]^{+\bullet}$, X-band EPR analysis in parallel mode was explored. Indeed, the signals at g_{eff} = 4.1 and 2.0 were significantly attenuated, while new broad resonances were observed at ca. 75 mT ($g \approx 9$) and at 150−250 mT (Figure 6a). The same behavior was observed for $[\mathbf{FeL^2Cl_2}]^{+\bullet}$, which also exhibited an intense resonance at 75 mT (Figure 6b). Such an intense signal at 75 mT has been previously reported for an octahedral Fe^{III}-phenoxyl radical complex, where the signal was attributed to the $|\Delta M_s|$ = 2 transition of a (S_{total} = 2) system arising from antiferromagnetic interactions between the ligand radical and Fe^{III} center.[10c] Thus, both $[\mathbf{FeL^1Cl}]^{+\bullet}$ and $[\mathbf{FeL^2Cl_2}]^{+\bullet}$ are tentatively assigned as integer spin systems by EPR that arise from antiferromagnetic interactions between the phenoxyl radical (S = 1/2) and the high spin Fe^{III} (S = 5/2) center.

3.8. Theoretical Analysis of $[\mathbf{FeL^1Cl}]^{+\bullet}$ and $[\mathbf{FeL^2Cl_2}]^{+\bullet}$.

As their short half-lives precluded isolation of the one-electron oxidized species $[\mathbf{FeL^1Cl}]^{+\bullet}$ and $[\mathbf{FeL^2Cl_2}]^{+\bullet}$, DFT calculations were completed to provide valuable insight into their electronic structure. High spin (S = 3, ligand radical ferromagnetically coupled to the high spin Fe^{III} center) and broken symmetry (S = 2, ligand radical antiferromagnetically coupled to the high spin Fe^{III} center) solutions were considered. Using the B3LYP[24]/ TZVP[25] level of theory, the two spin states were found to be essentially isoenergetic for both complexes, with the broken symmetry solutions being slightly favored in both cases (0.03 and 0.7 kcal/mol for $[\mathbf{FeL^1Cl}]^{+\bullet}$ and $[\mathbf{FeL^2Cl_2}]^{+\bullet}$, respectively). In addition, the exchange coupling J was calculated using the Yamaguchi formula (eq 4), which is applicable for systems from the strong to weak exchange limit.[37]

$$J = -\frac{E_{HS} - E_{BS}}{\langle \hat{S}^2 \rangle_{HS} - \langle \hat{S}^2 \rangle_{BS}} \quad (4)$$

The computed exchange coupling were −2 cm^{-1} and −48 cm^{-1} for $[\mathbf{FeL^1Cl}]^{+\bullet}$ and $[\mathbf{FeL^2Cl_2}]^{+\bullet}$, respectively, corresponding to weak antiferromagnetic (S = 2) exchange interaction for these systems. The strength of coupling is reflected in the amount of overlap between a metal-based SOMO and a ligand-based SOMO, which were found to be 23% and 24% for $[\mathbf{FeL^1Cl}]^{+\bullet}$ (Figure 7) and $[\mathbf{FeL^2Cl_2}]^{+\bullet}$ (Figure 8), respectively.[28] For $[\mathbf{FeL^2Cl_2}]^{+\bullet}$, the Fe1−O1 bond distance was predicted to elongate in comparison to the neutral complex (Table 1). This is indicative of the formation of a neutral phenoxyl radical upon oxidation, which has decreased electron donating ability relative to the anionic phenoxide moiety

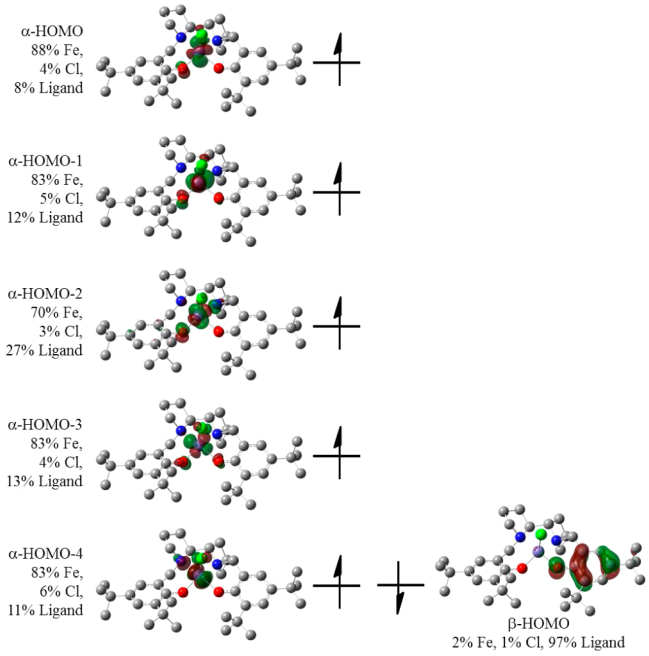

Figure 7. Biorthogonalized Kohn−Sham molecular orbitals for the broken symmetry solution of $[\mathbf{FeL^1Cl}]^{+\bullet}$. AOMix MO breakdown in brackets; see Experimental Section for details.

dx.doi.org/10.1021/ic500663x | *Inorg. Chem.* 2014, 53, 5810−5819

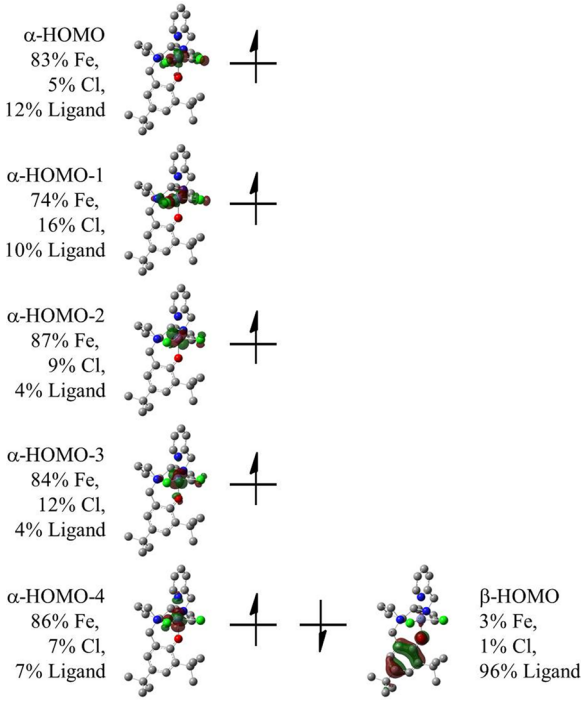

Figure 8. Biorthogonalized Kohn–Sham molecular orbitals for the broken symmetry solution of $[\mathbf{FeL^2Cl_2}]^{+\bullet}$. AOMix MO breakdown in brackets; see Experimental Section for details.

($\mathbf{FeL^2Cl_2}$: Fe–O 1.859 Å; $[\mathbf{FeL^2Cl_2}]^{+\bullet}$: Fe–O 2.014 Å). Additionally, the C–O bond distances of phenoxide/phenoxyl moieties are often indicative of the oxidation state of the ligand due to the formation of a quinoidal ring system upon oxidation. In this case, a shortening of the C–O bond was predicted upon oxidation ($\mathbf{FeL^2Cl_2}$: 1.332 Å; $[\mathbf{FeL^2Cl_2}]^{+\bullet}$: 1.276 Å), once again suggesting the formation of a ligand radical species (Table 1).

A similar pattern was observed for $[\mathbf{FeL^1Cl}]^{+\bullet}$. Interestingly, the electronic structure was predicted to contain a localized phenoxyl radical coupled to the Fe^{III} center and is highlighted by the predicted changes in C1–O1 ($\mathbf{FeL^1Cl}$: 1.340 Å; $[\mathbf{FeL^1Cl}]^{+\bullet}$: 1.347 Å) and C2–O2 bond distances ($\mathbf{FeL^1Cl}$: 1.335 Å; $[\mathbf{FeL^1Cl}]^{+\bullet}$: 1.278 Å). The shortening of the C2–O2 bond distance signifies phenoxyl radical formation on the ring system containing C2–O2, while the C1–O1 ring remains unchanged.

The formation of a localized phenoxyl radical in this symmetric system concurs with the moderate coupling observed by CV (K_c value), which has been used previously to evaluate the degree of delocalization for oxidized bisphenoxide complexes.[6f,i,l] This localized ligand radical electronic structure matches the report by Fujii et al., in which the increased metal charge (Mn^{III}) leads to d-orbital contraction, limiting delocalization of the ligand radical over the salen ligand scaffold.[6k]

4. CONCLUSION

Iron complexes $\mathbf{FeL^1Cl}$ and $\mathbf{FeL^2Cl_2}$ were synthesized by reacting $FeCl_2$ with the corresponding symmetric bisphenolate ($\mathbf{H_2L^1}$) and dissymmetric monophenolate ($\mathbf{HL^2}$) ligands in air. The synthetic strategy to the ligand $\mathbf{HL^2}$ can be generalized for the synthesis of other dissymmetric ligands employing the bipyrrolidine backbone. The electrochemistry of $\mathbf{FeL^1Cl}$ and $\mathbf{FeL^2Cl_2}$ displayed quasi-reversible redox waves corresponding to the number of redox-active phenoxides in the complex. Both complexes were shown to undergo clean one-electron oxidation using a suitable chemical oxidant as measured by UV–vis-NIR spectroscopy to afford $[\mathbf{FeL^1Cl}]^{+\bullet}$ and $[\mathbf{FeL^2Cl_2}]^{+\bullet}$. The locus of oxidation was demonstrated to be ligand-based by resonance Raman spectroscopy with the emergence of the ν_{7a} phenoxyl radical band. This formulation was well supported by EPR spectroscopy and theoretical studies, which further revealed the oxidized species contain a phenoxyl radical antiferromagnetically coupled to the high spin Fe^{III} center. Work involving the replacement of the chloride ligands to promote catalytic oxidation reactions is currently ongoing.

■ ASSOCIATED CONTENT

Ⓢ Supporting Information

X-ray crystal structures of (*R*,*R*)-$\mathbf{FeL^1Cl}$ and (*R*,*R*)-$\mathbf{FeL^2Cl_2}$, and cif files of all structures, electrochemical data of $\mathbf{H_2L^1}$ and $\mathbf{HL^2}$, X-band EPR spectra of the neutral and one-electron oxidized species, and further computational data. This material is available free of charge via the Internet at http://pubs.acs.org.

■ AUTHOR INFORMATION

Corresponding Author

*E-mail: tim_storr@sfu.ca.

Notes

The authors declare no competing financial interest.

■ ACKNOWLEDGMENTS

This work is supported by a NSERC Discovery Grant (T.S.), and a travel grant from the France-Canada Research Fund (T.S. and F.T.). L.C. thanks NSERC for a Research Exchange Travel Award. Compute Canada and Westgrid are acknowledged for access to computational resources. Brian O. Patrick is thanked for X-ray analysis of (*R*,*R*)-$\mathbf{FeL^2Cl_2}$.

■ REFERENCES

(1) (a) Stubbe, J. A.; van der Donk, W. A. *Chem. Rev.* **1998**, *98*, 2661–2661. (b) Whittaker, J. W. *Chem. Rev.* **2003**, *103*, 2347–2363.

(2) (a) Atienza, C. C. H.; Milsmann, C.; Lobkovsky, E.; Chirik, P. J. *Angew. Chem., Int. Ed.* **2011**, *50*, 8143–8147. (b) McNamara, W. R.; Han, Z.; Alperin, P. J.; Brennessel, W. W.; Holland, P. L.; Eisenberg, R. *J. Am. Chem. Soc.* **2011**, *133*, 15368–15371. (c) Russell, S. K.; Lobkovsky, E.; Chirik, P. J. *J. Am. Chem. Soc.* **2011**, *133*, 8858–8861. (d) Chirik, P. J. *Inorg. Chem.* **2011**, *50*, 9737–9740. (e) Chirik, P. J.; Wieghardt, K. *Science* **2010**, *327*, 794–795. (f) Blackmore, K. J.; Lal, N.; Ziller, J. W.; Heyduk, A. F. *J. Am. Chem. Soc.* **2008**, *130*, 2728–2729. (g) Buttner, T.; Geier, J.; Frison, G.; Harmer, J.; Calle, C.; Schweiger, A.; Schonberg, H.; Grutzmacher, H. *Science* **2005**, *307*, 235–238. (h) Haneline, M. R.; Heyduk, A. F. *J. Am. Chem. Soc.* **2006**, *128*, 8410–8411. (i) Koenigsmann, M.; Donati, N.; Stein, D.; Schoenberg, H.; Harmer, J.; Sreekanth, A.; Gruetzmacher, H. *Angew. Chem., Int. Ed.* **2007**, *46*, 3567–3570. (j) Maire, P.; Konigsmann, M.; Sreekanth, A.; Harmer, J.; Schweiger, A.; Grutzmacher, H. *J. Am. Chem. Soc.* **2006**, *128*, 6578–6580. (k) Miyazato, Y.; Wada, T.; Tanaka, K. *Bull. Chem. Soc. Jpn.* **2006**, *79*, 745–747. (l) Ringenberg, M. R.; Kokatam, S. L.; Heiden, Z. M.; Rauchfuss, T. B. *J. Am. Chem. Soc.* **2008**, *130*, 788–789.

(3) Jazdzewski, B. A.; Tolman, W. B. *Coord. Chem. Rev.* **2000**, *200*, 633–685.

(4) (a) Pratt, R. C.; Stack, T. D. P. *Inorg. Chem.* **2005**, *44*, 2367–2375. (b) Pratt, R. C.; Stack, T. D. P. *J. Am. Chem. Soc.* **2003**, *125*, 8716–8717. (c) Wang, Y. D.; DuBois, J. L.; Hedman, B.; Hodgson, K. O.; Stack, T. D. P. *Science* **1998**, *279*, 537–540. (d) Shimazaki, Y.; Huth, S.; Odani, A.; Yamauchi, O. *Angew. Chem., Int. Ed.* **2000**, *39*, 1666–1667. (e) Shimazaki, Y.; Huth, S.; Hirota, S.; Yamauchi, O.

Inorg. Chim. Acta **2002**, *331*, 168−177. (f) Thomas, F.; Gellon, G.; Luneau, I. G.; Saint-Aman, E.; Pierre, J. L. *Angew. Chem., Int. Ed.* **2002**, *41*, 3047−3050. (g) Thomas, F.; Jarjayes, O.; Duboc, C.; Philouze, C.; Saint-Aman, E.; Pierre, J. L. *Dalton Trans.* **2004**, 2662−2669. (h) Halfen, J. A.; Jazdzewski, B. A.; Mahapatra, S.; Berreau, L. M.; Wilkinson, E. C.; Que, L.; Tolman, W. B. *J. Am. Chem. Soc.* **1997**, *119*, 8217−8227. (i) Michel, F.; Thomas, F.; Hamman, S.; Philouze, C.; Saint-Aman, E.; Pierre, J.-L. *Eur. J. Inorg. Chem.* **2006**, 3684−3696. (j) Sokolowski, A.; Leutbecher, H.; Weyhermuller, T.; Schnepf, R.; Both, E.; Bill, E.; Hildebrandt, P.; Wieghardt, K. *J. Biol. Inorg. Chem.* **1997**, *2*, 444−453. (k) Zurita, D.; Menage, S.; Pierre, J. L.; SaintAman, E. *New J. Chem.* **1997**, *21*, 1001−1008. (l) Chaudhuri, P.; Hess, M.; Florke, U.; Wieghardt, K. *Angew. Chem., Int. Ed.* **1998**, *37*, 2217−2220. (m) Chaudhuri, P.; Hess, M.; Muller, J.; Hildenbrand, K.; Bill, E.; Weyhermuller, T.; Wieghardt, K. *J. Am. Chem. Soc.* **1999**, *121*, 9599−9610. (n) Itoh, S.; Taki, M.; Takayama, S.; Nagatomo, S.; Kitagawa, T.; Sakurada, N.; Arakawa, R.; Fukuzumi, S. *Angew. Chem., Int. Ed.* **1999**, *38*, 2774−2776. (o) Saint-Aman, E.; Menage, S.; Pierre, J. L.; Defrancq, E.; Gellon, G. *New J. Chem.* **1998**, *22*, 393−394. (p) Benisvy, L.; Blake, A. J.; Collison, D.; Davies, E. S.; Garner, C. D.; McInnes, E. J. L.; McMaster, J.; Whittaker, G.; Wilson, C. *Chem. Commun.* **2001**, 1824−1825. (q) Taki, M.; Hattori, H.; Osako, T.; Nagatomo, S.; Shiro, M.; Kitagawa, T.; Itoh, S. *Inorg. Chim. Acta* **2004**, *357*, 3369−3381. (r) Taki, M.; Kumei, H.; Itoh, S.; Fukuzumi, S. *J. Inorg. Biochem.* **2000**, *78*, 1−5. (s) Vaidyanathan, M.; Palaniandavar, M.; Gopalan, R. S. *Ind. J. Chem., Sect. A* **2003**, *42*, 2210−2222. (t) Zueva, E.; Walton, P. H.; McGrady, J. E. *Dalton Trans.* **2006**, 159−167.

(5) (a) Rodriguez-Lopez, J. N.; Hernandez-Ruiz, J.; Garcia-Canovas, F.; Thorneley, R. N. F.; Acosta, M.; Arnao, M. B. *J. Biol. Chem.* **1997**, *272*, 5469−5476. (b) Veitch, N. C. *Phytochemistry* **2004**, *65*, 249−259. (c) Jakopitsch, C.; Vlasits, J.; Wiseman, B.; Loewen, P. C.; Obinger, C. *Biochemistry* **2007**, *46*, 1183−1193. (d) Rittle, J.; Green, M. T. *Science* **2010**, *330*, 933−937.

(6) (a) Storr, T.; Wasinger, E. C.; Pratt, R. C.; Stack, T. D. P. *Angew. Chem., Int. Ed.* **2007**, *46*, 5198−5201. (b) Storr, T.; Verma, P.; Pratt, R. C.; Wasinger, E. C.; Shimazaki, Y.; Stack, T. D. P. *J. Am. Chem. Soc.* **2008**, *130*, 15448−15459. (c) Rotthaus, O.; Jarjayes, O.; Thomas, F.; Philouze, C.; Del Valle, C. P.; Saint-Aman, E.; Pierre, J. L. *Chem.—Eur. J.* **2006**, *12*, 2293−2302. (d) Rotthaus, O.; Jarjayes, O.; Del Valle, C. P.; Philouze, C.; Thomas, F. *Chem. Commun.* **2007**, 4462−4464. (e) Rotthaus, O.; Thomas, F.; Jarjayes, O.; Philouze, C.; Saint-Aman, E.; Pierre, J.-L. *Chem.—Eur. J.* **2006**, *12*, 6953−6962. (f) Shimazaki, Y.; Stack, T. D. P.; Storr, T. *Inorg. Chem.* **2009**, *48*, 8383−8392. (g) Orio, M.; Philouze, C.; Jarjayes, O.; Neese, F.; Thomas, F. *Inorg. Chem.* **2010**, *49*, 646−658. (h) Orio, M.; Jarjayes, O.; Kanso, H.; Philouze, C.; Neese, F.; Thomas, F. *Angew. Chem., Int. Ed.* **2010**, *49*, 4989−4992. (i) Chiang, L.; Kochem, A.; Jarjayes, O.; Dunn, T. J.; Vezin, H.; Sakaguchi, M.; Ogura, T.; Orio, M.; Shimazaki, Y.; Thomas, F.; Storr, T. *Chem.—Eur. J.* **2012**, *18*, 14117−14127. (j) Rotthaus, O.; Jarjayes, O.; Philouze, C.; Del Valle, C. P.; Thomas, F. *Dalton Trans.* **2009**, 1792−1800. (k) Kurahashi, T.; Fujii, H. *J. Am. Chem. Soc.* **2011**, *133*, 8307−8316. (l) Shimazaki, Y.; Arai, N.; Dunn, T. J.; Yajima, T.; Tani, F.; Ramogida, C. F.; Storr, T. *Dalton Trans.* **2011**, *40*, 2469−2479. (m) Kochem, A.; Kanso, H.; Baptiste, B.; Arora, H.; Philouze, C.; Jarjayes, O.; Vezin, H.; Luneau, D.; Orio, M.; Thomas, F. *Inorg. Chem.* **2012**, *51*, 10557−10571. (n) Kochem, A.; Jarjayes, O.; Baptiste, B.; Philouze, C.; Vezin, H.; Tsukidate, K.; Tani, F.; Orio, M.; Shimazaki, Y.; Thomas, F. *Chem.—Eur. J.* **2012**, *18*, 1068−1072. (o) Verma, P.; Pratt, R. C.; Storr, T.; Wasinger, E. C.; Stack, T. D. P. *Proc. Natl. Acad. Sci. U.S.A.* **2011**, *108*, 18600−18605. (p) de Bellefeuille, D.; Askari, M. S.; Lassalle-Kaiser, B.; Journaux, Y.; Aukauloo, A.; Orio, M.; Thomas, F.; Ottenwaelder, X. *Inorg. Chem.* **2012**, *51*, 12796−12804. (q) Asami, K.; Tsukidate, K.; Iwatsuki, S.; Tani, F.; Karasawa, S.; Chiang, L.; Storr, T.; Thomas, F.; Shimazaki, Y. *Inorg. Chem.* **2012**, *51*, 12450−12461. (r) Pratt, R. C.; Lyons, C. T.; Wasinger, E. C.; Stack, T. D. P. *J. Am. Chem. Soc.* **2012**, *134*, 7367−7377.

(7) (a) Canali, L.; Sherrington, D. C. *Chem. Soc. Rev.* **1999**, *28*, 85−93. (b) Darensbourg, D. J. *Chem. Rev.* **2007**, *107*, 2388−2410. (c) Irie, R.; Noda, K.; Ito, Y.; Matsumoto, N.; Katsuki, T. *Tetrahedron Lett.* **1990**, *31*, 7345−7348. (d) Jacobsen, E. N.; Zhang, W.; Muci, A. R.; Ecker, J. R.; Deng, L. *J. Am. Chem. Soc.* **1991**, *113*, 7063−7064. (e) McGarrigle, E. M.; Gilheany, D. G. *Chem. Rev.* **2005**, *105*, 1563−1602.

(8) Kurahashi, T.; Kobayashi, Y.; Nagatomo, S.; Tosha, T.; Kitagawa, T.; Fujii, H. *Inorg. Chem.* **2005**, *44*, 8156−8166.

(9) (a) Wollmann, R. G.; Hendrickson, D. N. *Inorg. Chem.* **1977**, *16*, 723−733. (b) Nairn, A. K.; Bhalla, R.; Foxon, S. P.; Liu, X. M.; Yellowlees, L. J.; Gilbert, B. C.; Walton, P. H. *J. Chem. Soc., Dalton Trans.* **2002**, 1253−1255. (c) Floquet, S.; Ottenwaelder, X.; Boillot, M.-L. *Inorg. Chem. Commun.* **2007**, *10*, 1549−1553. (d) Strautmann, J. B. H.; George, S. D.; Bothe, E.; Bill, E.; Weyhermueller, T.; Stammler, A.; Boegge, H.; Glaser, T. *Inorg. Chem.* **2008**, *47*, 6804−6824. (e) Bottcher, A.; Grinstaff, M. W.; Labinger, J. A.; Gray, H. B. *J. Mol. Catal. A: Chem.* **1996**, *113*, 191−200. (f) Bryliakov, K. P.; Talsi, E. P. *Angew. Chem., Int. Ed.* **2004**, *43*, 5228−5230. (g) Sivasubramanian, V. K.; Ganesan, M.; Rajagopal, S.; Ramaraj, R. *J. Org. Chem.* **2002**, *67*, 1506−1514.

(10) (a) Adam, B.; Bill, E.; Bothe, E.; Goerdt, B.; Haselhorst, G.; Hildenbrand, K.; Sokolowski, A.; Steenken, S.; Weyhermuller, T.; Wieghardt, K. *Chem.—Eur. J.* **1997**, *3*, 308−319. (b) Snodin, M. D.; Ould-Moussa, L.; Wallmann, U.; Lecomte, S.; Bachler, V.; Bill, E.; Hummel, H.; Weyhermuller, T.; Hildebrandt, P.; Wieghardt, K. *Chem.—Eur. J.* **1999**, *5*, 2554−2565. (c) Kimura, S.; Bill, E.; Bothe, E.; Weyhermuller, T.; Wieghardt, K. *J. Am. Chem. Soc.* **2001**, *123*, 6025−6039. (d) Allard, M. M.; Sonk, J. A.; Heeg, M. J.; McGarvey, B. R.; Schlegel, H. B.; Verani, C. N. *Angew. Chem., Int. Ed.* **2012**, *51*, 3178−3182. (e) Lanznaster, M.; Hratchian, H. P.; Heeg, M. J.; Hryhorczuk, L. M.; McGarvey, B. R.; Schlegel, H. B.; Verani, C. N. *Inorg. Chem.* **2006**, *45*, 955−957.

(11) Mayilmurugan, R.; Sankaralingam, M.; Suresh, E.; Palaniandavar, M. *Dalton Trans.* **2010**, *39*, 9611−9625.

(12) Hasan, K.; Fowler, C.; Kwong, P.; Crane, A. K.; Collins, J. L.; Kozak, C. M. *Dalton Trans.* **2008**, 2991−2998.

(13) Kirillov, E.; Lavanant, L.; Thomas, C.; Roisnel, T.; Chi, Y.; Carpentier, J.-F. *Chem.—Eur. J.* **2007**, *13*, 923−935.

(14) (a) Sergeeva, E.; Kopilov, J.; Goldberg, I.; Kol, M. *Inorg. Chem.* **2009**, *48*, 8075−8077. (b) Sergeeva, E.; Kopilov, J.; Goldberg, I.; Kol, M. *Chem. Commun.* **2009**, 3053−3055. (c) Sergeeva, E.; Press, K.; Goldberg, I.; Kol, M. *Eur. J. Inorg. Chem.* **2013**, 3362−3369.

(15) (a) Suzuki, K.; Oldenburg, P. D.; Que, L., Jr. *Angew. Chem., Int. Ed.* **2008**, *47*, 1887−1889. (b) Chen, M. S.; White, M. C. *Science* **2007**, *318*, 783−787. (c) Chen, M. S.; White, M. C. *Science* **2010**, *327*, 566−571. (d) Gormisky, P. E.; White, M. C. *J. Am. Chem. Soc.* **2013**, *135*, 14052−14055. (e) Cusso, O.; Garcia-Bosch, I.; Ribas, X.; Lloret-Fillol, J.; Costas, M. *J. Am. Chem. Soc.* **2013**, *135*, 14871−14878.

(16) Perrin, D. D.; Armarego, W. L. F. *Purification of Laboratory Chemicals*, 1st ed.; Pergamo Press: New York, 1988.

(17) (a) Bjorn, A. Thesis, University of Cincinnati, Cincinnati, OH, 2002. (b) Murata, Y.; Cheng, F.; Kitagawa, T.; Komatsu, K. *J. Am. Chem. Soc.* **2004**, *126*, 8874−8875.

(18) (a) Cepanec, I.; Mikuldas, H.; Vinkovic, V. *Synth. Commun.* **2001**, *31*, 2913−2919. (b) Wong, Y.-L.; Tong, L. H.; Dilworth, J. R.; Ng, D. K. P.; Lee, H. K. *Dalton Trans.* **2010**, *39*, 4602−4611.

(19) Altomare, A.; Burla, M. C.; Camalli, M.; Cascarano, G. L.; Giacovazzo, C.; Guagliardi, A.; Moliterni, A. G. G.; Polidori, G.; Spagna, R. *J. Appl. Crystallogr.* **1999**, *32*, 115−119.

(20) Betteridge, P. W.; Carruthers, J. R.; Cooper, R. I.; Prout, K.; Watkin, D. J. *J. Appl. Crystallogr.* **2003**, *36*, 1487−1487.

(21) Huebschle, C. B.; Sheldrick, G. M.; Dittrich, B. *J. Appl. Crystallogr.* **2011**, *44*, 1281−1284.

(22) *Persistence of Vision Raytracer (POV-Ray)*, 3.6.2; Persistence of Vision Pty. Ltd.: Victoria, Australia, 2004.

(23) Frisch, M. J.; Trucks, G. W.; Schlegel, H. B.; Scuseria, G. E.; Robb, M. A.; Cheeseman, J. R.; Scalmani, G.; Barone, V.; Mennucci, B.; Petersson, G. A.; Nakatsuji, H.; Caricato, M.; Li, X.; Hratchian, H. P.; Izmaylov, A. F.; Bloino, J.; Zheng, G.; Sonnenberg, J. L.; Hada, M.; Ehara, M.; Toyota, K.; Fukuda, R.; Hasegawa, J.; Ishida, M.; Nakajima, T.; Honda, Y.; Kitao, O.; Nakai, H.; Vreven, T.; Montgomery, J. A., Jr.;

Peralta, J. E.; Ogliaro, F.; Bearpark, M.; Heyd, J. J.; Brothers, E.; Kudin, K. N.; Staroverov, V. N.; Kobayashi, R.; Normand, J.; Raghavachari, K.; Rendell, A.; Burant, J. C.; Iyengar, S. S.; Tomasi, J.; Cossi, M.; Rega, N.; Millam, N. J.; Klene, M.; Knox, J. E.; Cross, J. B.; Bakken, V.; Adamo, C.; Jaramillo, J.; Gomperts, R.; Stratmann, R. E.; Yazyev, O.; Austin, A. J.; Cammi, R.; Pomelli, C.; Ochterski, J. W.; Martin, R. L.; Morokuma, K.; Zakrzewski, V. G.; Voth, G. A.; Salvador, P.; Dannenberg, J. J.; Dapprich, S.; Daniels, A. D.; Farkas, Ö.; Foresman, J. B.; Ortiz, J. V.; Cioslowski, J.; Fox, D. J. *Gaussian 09, Revision D.01*, Gaussian, Inc.: Wallingford CT, 2009.

(24) (a) Becke, A. D. *J. Chem. Phys.* **1993**, *98*, 5648−5652. (b) Stephens, P. J.; Devlin, F. J.; Chabalowski, C. F.; Frisch, M. J. *J. Phys. Chem.* **1994**, *98*, 11623−11627.

(25) (a) Schafer, A.; Horn, H.; Ahlrichs, R. *J. Chem. Phys.* **1992**, *97*, 2571−2577. (b) Schafer, A.; Huber, C.; Ahlrichs, R. *J. Chem. Phys.* **1994**, *100*, 5829−5835.

(26) (a) Noodleman, L. *J. Chem. Phys.* **1981**, *74*, 5737−5743. (b) Noodleman, L.; Davidson, E. R. *Chem. Phys.* **1986**, *109*, 131−143. (c) Noodleman, L.; Case, D. A. *Adv. Inorg. Chem.* **1992**, *38*, 423−+.

(27) (a) Herebian, D.; Wieghardt, K. E.; Neese, F. *J. Am. Chem. Soc.* **2003**, *125*, 10997−11005. (b) Neese, F. *J. Phys. Chem. Solids* **2004**, *65*, 781−785.

(28) (a) Gorelsky, S. I. *AOMix, Program for Molecular Orbital Analysis*, version 6.85; 2014. http://www.sg-chem.net/. (b) Gorelsky, S. I.; Lever, A. B. P. *J. Organomet. Chem.* **2001**, *635*, 187−196. (c) Gorelsky, S. I.; Solomon, E. I. *Theor. Chem. Acc.* **2008**, *119*, 57−67.

(29) Alexakis, A.; Tomassini, A.; Chouillet, C.; Roland, S.; Mangeney, P.; Bernardinelli, G. *Angew. Chem., Int. Ed.* **2000**, *39*, 4093−4095.

(30) (a) Fujii, H.; Funahashi, Y. *Angew. Chem., Int. Ed.* **2002**, *41*, 3638−3641. (b) Kurahashi, T.; Oda, K.; Sugimoto, M.; Ogura, T.; Fujii, H. *Inorg. Chem.* **2006**, *45*, 7709−7721.

(31) Addison, A. W.; Rao, T. N.; Reedijk, J.; Vanrijn, J.; Verschoor, G. C. *J. Chem. Soc., Dalton Trans.* **1984**, 1349−1356.

(32) (a) Ganzenmuller, G.; Berkaine, N.; Fouqueau, A.; Casida, M. E.; Reiher, M. *J. Chem. Phys.* **2005**, *122*, No. 234321. (b) Pierloot, K.; Vancoillie, S. *J. Chem. Phys.* **2008**, *128*, No. 204109. (c) Reiher, M.; Salomon, O.; Hess, B. A. *Theor. Chem. Acc.* **2001**, *107*, 48−55.

(33) (a) Collins, M. J.; Ray, K.; Que, L., Jr. *Inorg. Chem.* **2006**, *45*, 8009−8011. (b) Sastri, C. V.; Lee, J.; Oh, K.; Lee, Y. J.; Lee, J.; Jackson, T. A.; Ray, K.; Hirao, H.; Shin, W.; Halfen, J. A.; Kim, J.; Que, L., Jr.; Shaik, S.; Nam, W. *Proc. Natl. Acad. Sci. U.S.A.* **2007**, *104*, 19181−19186. (c) Que, L., Jr. *Acc. Chem. Res.* **2007**, *40*, 493−500. (d) Wang, D.; Farquhar, E. R.; Stubna, A.; Munck, E.; Que, L., Jr. *Nat. Chem.* **2009**, *1*, 145−150. (e) Wang, D.; Ray, K.; Collins, M. J.; Farquhar, E. R.; Frisch, J. R.; Gomez, L.; Jackson, T. A.; Kerscher, M.; Waleska, A.; Comba, P.; Costas, M.; Que, L., Jr. *Chem. Sci.* **2013**, *4*, 282−291. (f) Lee, Y.-M.; Kotani, H.; Suenobu, T.; Nam, W.; Fukuzumi, S. *J. Am. Chem. Soc.* **2008**, *130*, 434−435.

(34) Flanagan, J. B.; Margel, S.; Bard, A. J.; Anson, F. C. *J. Am. Chem. Soc.* **1978**, *100*, 4248−4253.

(35) Patterson, A.; Storr, T. Simon Fraser University, 2014, unpublished results.

(36) Schnepf, R.; Sokolowski, A.; Muller, J.; Bachler, V.; Wieghardt, K.; Hildebrandt, P. *J. Am. Chem. Soc.* **1998**, *120*, 2352−2364.

(37) (a) Yamaguchi, K.; Takahara, Y.; Fueno, T. *Applied Quantum Chemistry*; Smith, V. H., Ed.; Reidel: Dordrecht, 1986. (b) Soda, T.; Kitagawa, Y.; Onishi, T.; Takano, Y.; Shigeta, Y.; Nagao, H.; Yoshioka, Y.; Yamaguchi, K. *Chem. Phys. Lett.* **2000**, *319*, 223−230.